Hindawi
International Journal of Antennas and Propagation
Volume 2017, Article ID 1691580, 13 pages
https://doi.org/10.1155/2017/1691580

Research Article

On the Design of Conical Antennas for Broadband Impedance Matching Performance

Francisco Estêvão Simão Pereira and Maurício Henrique Costa Dias

Military Institute of Engineering, 22290-270 Rio de Janeiro, RJ, Brazil

Correspondence should be addressed to Maurício Henrique Costa Dias; mhcdias@ime.eb.br

Received 29 December 2016; Accepted 7 February 2017; Published 27 February 2017

Academic Editor: Ikmo Park

In the scope of broadband radiators, the biconical antenna, or its monopole conical counterpart, is long known to be a proper choice. One common form of such radiator, the spherically capped conical antenna (SCCA), has closed-form solution to its input impedance, from which the broadband performance potential is easily verified. Nonetheless, from the design perspective, apart from a few clues inferred from existing solutions, little is found to accurately guide the choice of the main geometrical parameters of the antenna that will enable it to comply with a set of imposed bandwidth requirements. This paper proposes a simple 10-step sequence to derive conical or biconical antenna design charts. These charts provide straightforward information on the geometrical limits within which the required antenna impedance matching broadband performance is achieved. The method is assessed for the SCCA and the open conical antenna (OCA) using theoretical and simulated estimates of the input impedance. A discussion on the impact of the cap and the feed gap is included.

1. Introduction

Biconical and conical antennas are among the most widely known radiators. They are natural choices for RF communication, broadcasting, or EMI testing, whenever omnidirectional radiation pattern and broadband performance are needed. The basic conical geometry (or biconical in its dipole equivalent) is typically assembled either by a wire grid or by a continuous metal surface [1, 2].

The ideal biconical geometry is actually a frequency-independent antenna, though it is not a feasible one, since it extends to infinity in the axial direction. Its input impedance does not change with frequency. Realistic biconical antennas must be truncated, leading to a broadband rather than frequency-independent response [1, 2].

Truncated versions of the biconical and conical antenna have been addressed as early as the 1940s by Schelkunoff [3], Smith [4] and Papas and King [5, 6], providing analytic approaches to calculate the antenna impedance and field pattern dependence on frequency and on the main geometric parameters (length and flare angle). Those antennas have still drawn attention through the following decades up to the present days. Recent analytical works on the subject may be found, for instance, in [7–9]. Nevertheless, information regarding the design point of view of such antennas, as in [10], for instance, is still scarce in the literature, especially when specific broadband performance criteria must be fulfilled.

A typical question that may arise for the designer of such antenna is how its geometric parameters should be chosen from start. Yet, how can one combine compactness and broadband performance up to the required levels considering such a structure? Though a few clues may be inferred from the mere observation of commercially available antennas, reliable open-source information to accurately aid the antenna engineer in this sense is not easily found.

In the present scope, this work discusses a simple method to derive bandwidth compliance charts for the design of conical and biconical antennas. These design charts set the limits that the main geometric parameters must fall within so that the antenna should be able to comply with a given imposed bandwidth constraint. The method is easily applied to any variant of the conical or biconical antenna, provided that a

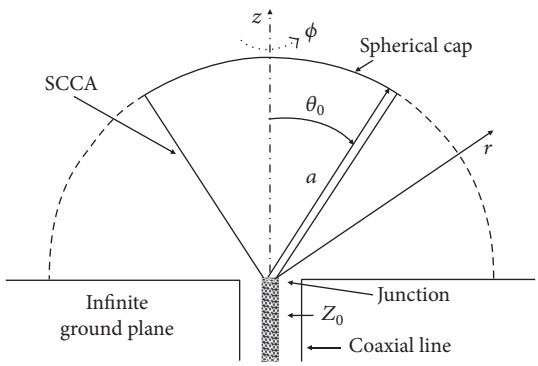

Figure 1: Vertical plane cut of an SCCA fed by a coaxial feed line. The antenna is a body of revolution over the z-axis.

series of impedance estimates spanning a frequency band large enough and some different flare angle values is obtained. Such estimates may be derived analytically, for instance, when closed-form equations are available, as in the case of the spherically capped conical antenna (SCCA) addressed in [5]. Otherwise, they can be collected by measurements or computed with the aid of antenna analysis tools, such as CST MW Studio, FEKO, HFSS, and NEC implementations. In this work, focus is given to the SCCA and to the open conical antenna (OCA), first analytically for the former, then with data generated by CST MW Studio for both of them. The influence of the cap and the feed gap is also discussed.

Section 2 summarizes the theoretical approach of Papas and King [5] on the SCCA, providing further insight on its bandwidth performance, from the antenna designer perspective. The method to derive design charts for broadband performance is described in the following section, taking as reference the design of an SCCA to be broadband matched to a 50 Ω load. Section 4 applies the proposed method to derive charts for the design of an OCA matched to 50 Ω, using impedance estimates calculated by simulation on CST MW Studio. Both SCCA and OCA bandwidth performances are analyzed, taking into account also the cap and the feed gap impact. Section 5 concludes this paper.

2. SCCA Input Impedance

2.1. Theoretical Model. The reference antenna in the present work is the SCCA fed by a coaxial line depicted in Figure 1. The ground plane is supposed to be ideal, that is, infinitely extended. The cone and the ground plane are also assumed to be perfect electrical conductors (PEC). This conical antenna configuration was assessed by Papas and King in [5] to derive an equation of the input impedance Z_{in} of an antenna of length a and flare angle θ_0, leading to

$$Z_{\text{in}} = Z_0 \frac{1 - \beta/\alpha}{1 + \beta/\alpha}, \tag{1}$$

where

$$Z_0 = 60 \ln \cot\left(\frac{\theta_0}{2}\right), \tag{2}$$

$$\frac{\beta}{\alpha} = e^{-2ika} \cdot \frac{1 + i\left(60/Z_0\right) \sum_{n=1}^{\infty} \left((2n+1)/n(n+1)\right) \left[P_n\left(\cos\theta_0\right)\right]^2 \zeta_n(ka)}{1 - i\left(60/Z_0\right) \sum_{n=1}^{\infty} \left((2n+1)/n(n+1)\right) \left[P_n\left(\cos\theta_0\right)\right]^2 \zeta_n(ka)}, \tag{3}$$

$$\zeta_n(ka) = \frac{h_n^{(2)}(ka)}{h_{n-1}^{(2)}(ka) - (n/ka)\, h_n^{(2)}(ka)}, \tag{4}$$

$h_n^{(2)}$ is the spherical Hankel function of the second kind, and $P_n(\cos\theta_0)$ is the Legendre polynomial of order n. The summation in (3) must be over odd integral values. Yet, Z_0 is defined as the characteristic impedance of the antenna and ka is the wave number $k = 2\pi/\lambda = 2\pi f/c$ multiplied by the sphere radius or cone side length a (λ is the free-space wavelength, f the frequency, and c the speed of light in vacuum).

It must be remarked that (1) holds for any reference plane along the coaxial line, provided that its characteristic impedance is equal to the antenna's Z_0. Otherwise, (1) represents the impedance at the junction reference plane in Figure 1, and the proper correction factor must be applied at other reference planes along the cable, as addressed in [7].

If the biconical equivalent of the SCCA is to be analyzed instead, the set of equations (1) to (4) still holds, replacing (2) by

$$Z_0 = 120 \ln \cot\left(\frac{\theta_0}{2}\right). \tag{5}$$

Figure 2 illustrates $Z_{\text{in}} = R_{\text{in}} + iX_{\text{in}}$ as a function of ka for three different flare angles: 15°, 45°, and 75°. The summation in (3) was truncated with a relative error of 10^{-4}. The broadband potential is clear as the antenna is large (high a) or the frequency is high or both, since R_{in} converges to Z_0 while X_{in} converges to 0. It is also worth remarking how Z_0 decreases with θ_0 and how the damped oscillations are relatively high at the first two cycles. Such features are paramount from the design perspective, especially if antenna compactness is a major requirement.

2.2. Bandwidth Performance. A proper assessment of how broadband the antenna may be depends not only on the antenna impedance itself but also on the reference impedance Z_r to which it should be matched. Yet, it depends on a reflection coefficient (S_{11}) threshold, below which antenna matching is regarded as achieved for practical purposes. In this work, the reference impedance is $Z_r = 50\,\Omega$ and two S_{11} thresholds are considered: −6 and −10 dB. These values are typical samples of what is seen in commercial antenna brochures and in antenna literature in general for different target applications.

Figure 3 illustrates S_{11} for the same impedance responses plotted in Figure 2. The SCCA with 45° flare angle reaches the −6 dB threshold at $ka = 0.94$ and the −10 dB one at $ka = 1.2$. From those points on, the antenna is matched. It is expected that the best broadband performances be achieved for the flare angles providing Z_0 close to the 50 Ω reference impedance. Such will take place roughly for angles between 30° and 60° for the SCCA. Nonetheless, the 15° angle is

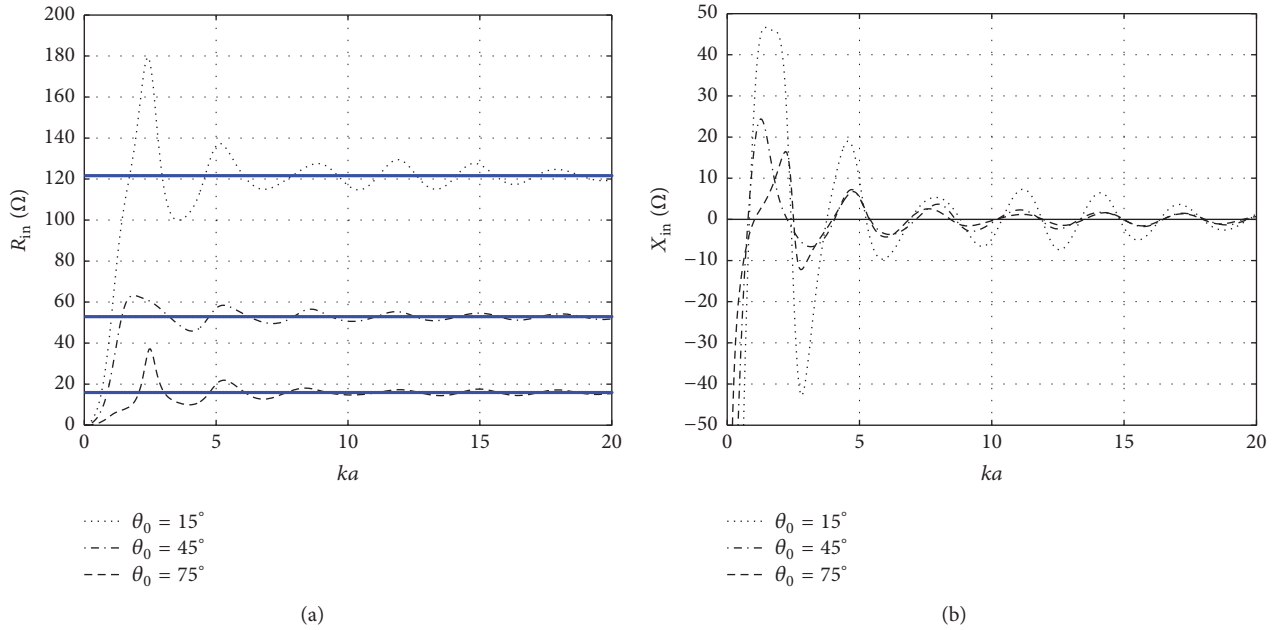

FIGURE 2: SCCA input impedance versus ka for $\theta_0 = 15^\circ$, 45°, and 75°: (a) resistance (R_{in}) and (b) reactance (X_{in}). Z_0 for each θ_0 is represented by a solid horizontal line in (a).

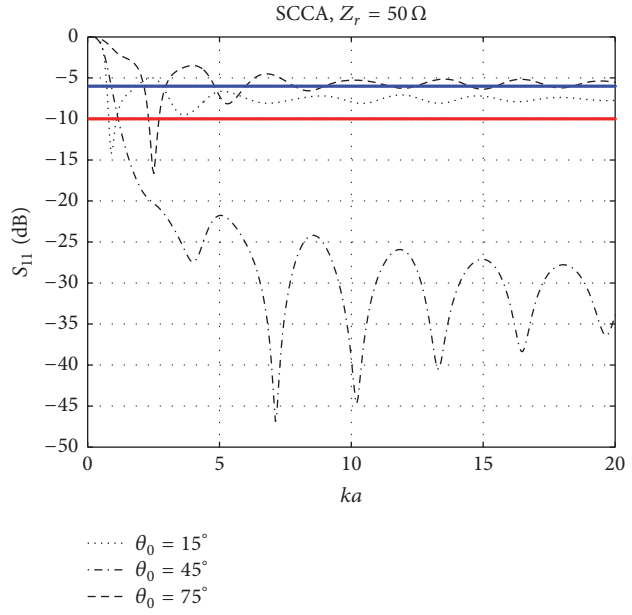

FIGURE 3: S_{11} of the SCCA versus ka for $\theta_0 = 15^\circ$, 45°, and 75° for $Z_r = 50\,\Omega$.

still able to provide broadband behavior from $ka = 2.88$ on, regarding the −6 dB limit, but it is not compliant with the more rigorous −10 dB level. On its turn, with $\theta_0 = 75^\circ$, the matching threshold would have to be as high as −3.5 dB for the antenna to present acceptable wideband matching from the second resonance on.

As expected from the damped oscillatory behavior of the SCCA impedance, the most critical region for achieving wideband matching is at the lowest values of ka. In this sense, the lowest impedance matching ka (ka_L) is a relevant parameter from the design point of view. In cases such as the 45° angle, though the bandwidth is theoretically unlimited, it has a starting point that defines the lowest operation frequency if the antenna length is fixed, or, alternatively, how small can the antenna length be, for a given desired lowest operation frequency.

To sum up, the antenna designer cannot rely exclusively on Z_0 to choose the geometric parameters. A closer look

to the first cycles of the impedance response is crucial to define the lowest operation limit. Furthermore, other practical aspects will result in changes both on the lowest and on the highest limits of the passband, requiring more realistic impedance estimates than the ones derived by Papas and King's model.

3. Design Chart for Broadband Performance

As addressed in the previous section, the broadband antenna design point of view goes beyond what is inferred from the impedance response alone. The impedance dependence on the antenna main geometrical parameters must be previously mapped and translated to bandwidth performance that must comply with imposed project requirements, expressed in terms of a reference impedance and reflection coefficient thresholds.

In this sense, a general method to derive bandwidth compliance charts to aid the conical or biconical antenna design is proposed step by step, as follows. It is explained taking the SCCA theoretical model briefly reproduced in Section 2 as reference but may easily be extended to other potentially broadband antennas, even if no analytical model is available to calculate its impedance. The method is exemplified with specific reference values while the sequence is chained.

(i) Calculate a reasonable number N of impedance responses within practical limits of the flare angle, say $N = 71$ responses from 10° to 80°, as considered in the present example.

(ii) From the design requirements, define the reference impedance ($Z_r = 50\,\Omega$, e.g., as considered in the present example) and calculate the corresponding S_{11} for the N impedance responses.

(iii) Yet, from the design requirements, define a reference passband threshold, say −6 or −10 dB, and a maximum ka of interest ($ka_{\max}$). Alternatively, for a given fixed a, the maximum frequency of interest $f_{\max}$ must be chosen. In the present example, both −6 and −10 dB are chosen.

(iv) Choose a criterion to define the lowest operation ka or frequency (ka_L or f_L, resp.). It can be the lowest ka or frequency that cuts the threshold (1st criterion) or the lowest ka or frequency of the largest observable subband (2nd criterion), as depicted in Figure 4. The former is chosen for the remainder of this work.

(v) Choose the bandwidth metric, which could be either the relative bandwidth BW_r or the ka_H/ka_L ratio (or f_H/f_L for a given fixed a). The latter is chosen for the present example. BW_r is computed as

$$\mathrm{BW}_r = 2\frac{ka_H - ka_L}{ka_H + ka_L}, \tag{6}$$

or for a given fixed a

$$\mathrm{BW}_r = 2\frac{f_H - f_L}{f_H + f_L}. \tag{7}$$

It is worth remarking that a common broadband criterion is that $\mathrm{BW}_r > 2/3$ or, equivalently, $f_H/f_L > 2$ [1, 2].

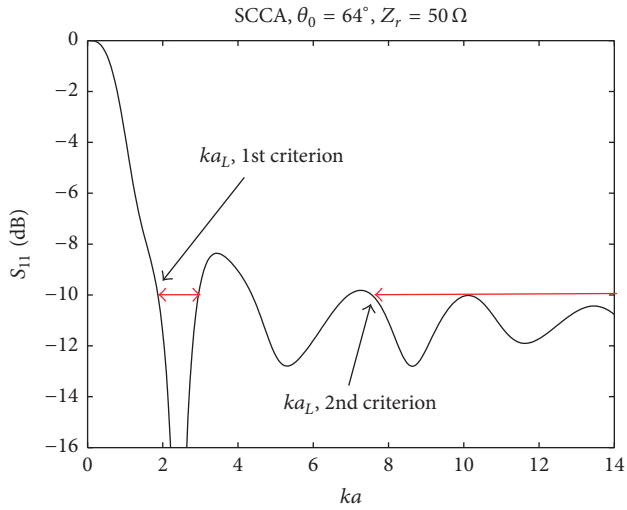

Figure 4: Lowest operation ka_L definition criteria.

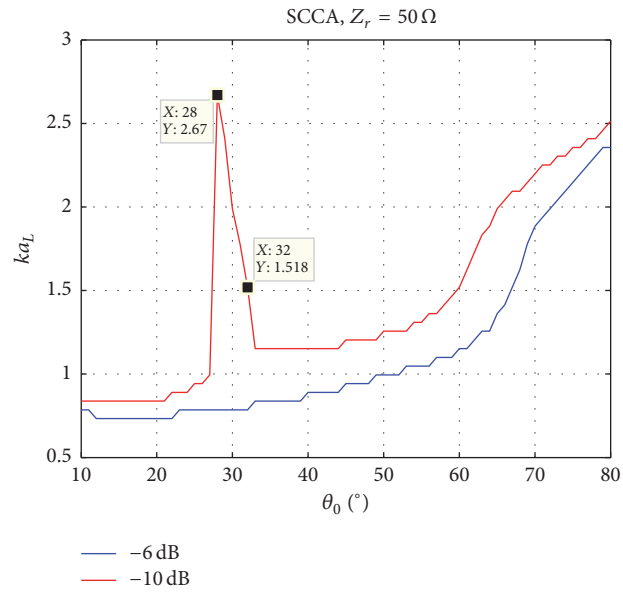

Figure 5: $ka_L \times \theta_0$ for the theoretical SCCA example.

(vi) For each of N S_{11} responses available, find ka_H and ka_L (or f_H and f_L for a given fixed a) that cross the reference S_{11} threshold.

(vii) Plot ka_L (or its normalized version $ka_L/2\pi = a_L/\lambda_L$) $\times\ \theta_0$, as illustrated in Figure 5 for this example. If a fixed length a is given, plot $f_L \times \theta_0$ instead. The apparently odd behavior of ka_L at 27–33° in Figure 5 is a mere consequence of S_{11} response of the present example, as seen in Figure 6.

(viii) Plot ka_H/ka_L (or f_H/f_L for a given fixed a) $\times\ \theta_0$. Figure 7 illustrates such a graph for the present example. It is worth remarking that ka_H is actually equal to $ka_{\max}$ in θ_0 range for which $ka_H/ka_L > 10$. This is a consequence of the convergence of the SCCA impedance to Z_0, as seen in Figures 2 and 3. In this example, $ka_{\max} = 52.36$, or equivalently $f_{\max} = 1$ GHz for $a = 2.5$ m. However, such behavior does not

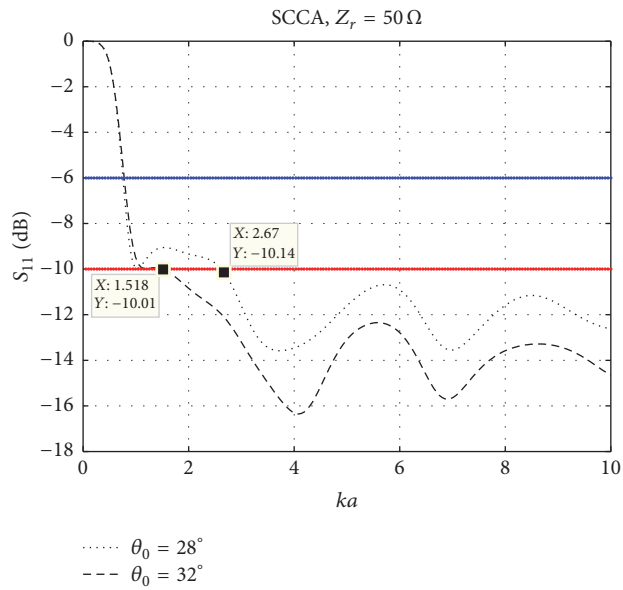

FIGURE 6: S_{11} of the theoretical SCCA example versus ka for $\theta_0 = 28^\circ$ and 32° for $Z_r = 50\,\Omega$.

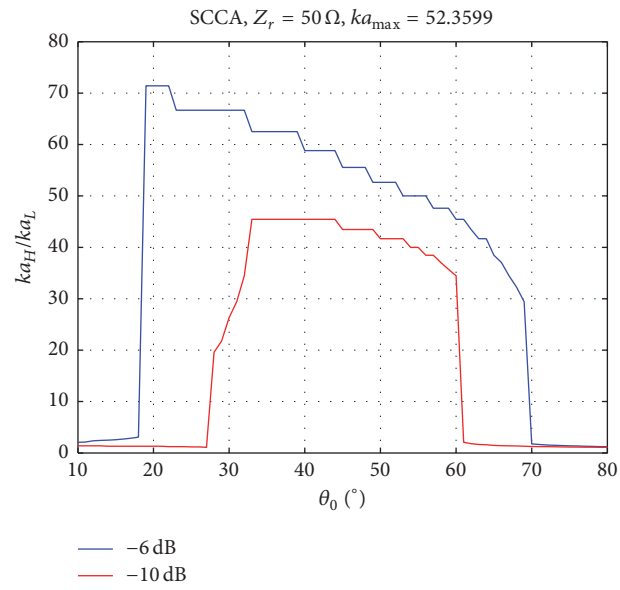

FIGURE 7: $ka_H/ka_L \times \theta_0$ for the theoretical SCCA example.

necessarily hold for more realistic impedance estimates, as discussed ahead in Section 4.

(ix) From the design requirements, define the minimum desired target for ka_H/ka_L ratio (or f_H/f_L for a given fixed a), $\mathrm{DF}_{\min}$, say $\mathrm{DF}_{\min} = 20$ for the present example.

(x) From the intermediary design charts $ka_L \times \theta_0$ and $ka_H/ka_L \times \theta_0$, generate a $M \times N$ truth table, M being a chosen number of samples of ka_L within expected values from the design requirements, where each cell is true whenever $ka_H/ka_L(ka_L, \theta_0) \geq \mathrm{DF}_{\min}$. This resulting matrix provides a chart like the one illustrated in Figure 8(a). The vertical axis is represented in terms of the normalized version of ka_L ($ka_L/2\pi = a/\lambda_L$, the relative length) in the example. Alternatively, instead of sampling ka_L, the length a may be sampled over $f_L \times \theta_0$ and $f_H/f_L \times \theta_0$ plots, resulting in a chart like the one in Figure 8(b). In this example, $f_L = 30$ MHz and $f_{\max} = 1$ GHz. This absolute version of the chart is actually the most helpful for the antenna design, providing straightforwardly the length and angle values for which the desired bandwidth performance is achieved, for a given set of requirements.

The specific results of this example show that the SCCA is able to provide 50 Ω broadband impedance matching even with lengths smaller than $\lambda_L/4$. For the −6 dB threshold, the

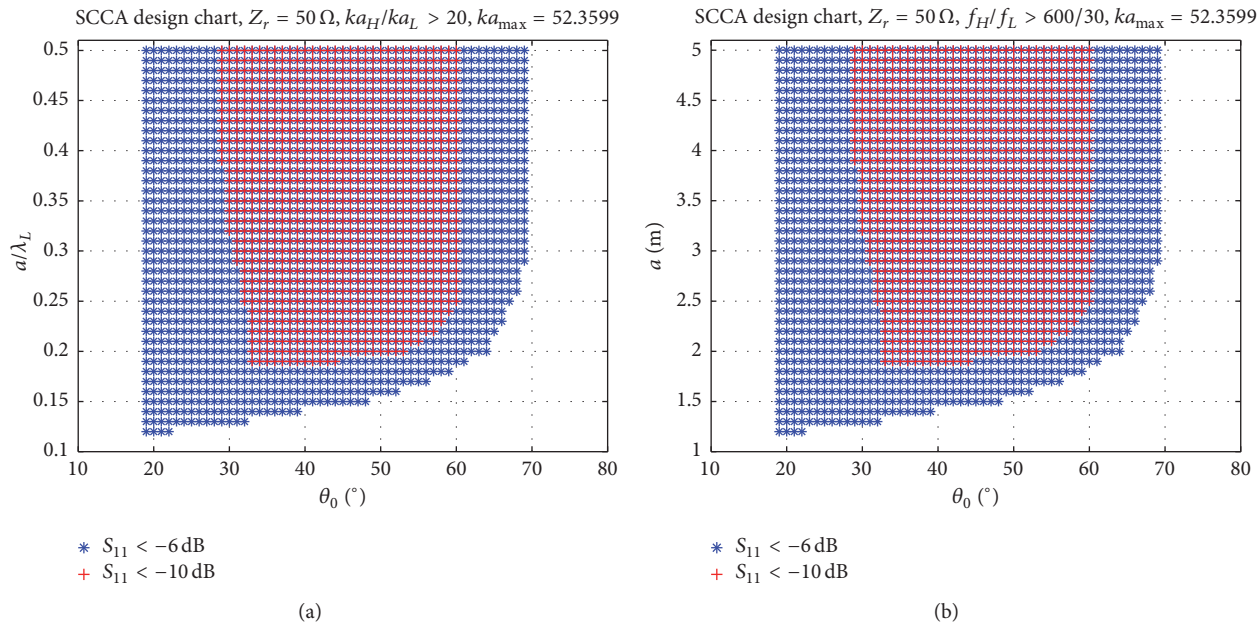

Figure 8: Design chart for the theoretical SCCA example with $DF_{min} = 20$: (a) relative and (b) absolute length versus θ_0.

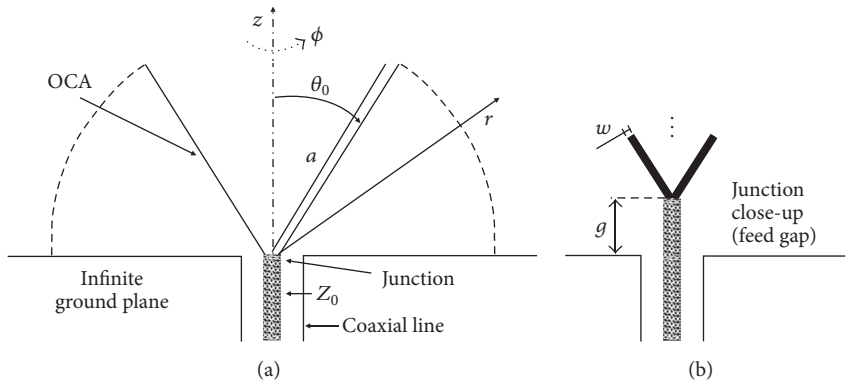

Figure 9: (a) Vertical plane cut of an OCA fed by a coaxial feed line and (b) a close-up of its junction. The antenna is a body of revolution over the z-axis.

length can be as small as $0.12\lambda_L$ and θ_0 as narrow as 19°, while for −10 dB the antenna must have at least $0.19\lambda_L$ and $\theta_0 = 33°$ to comply. A note is due regarding the biconical counterpart. Since its Z_0 is twice the value of the conical antenna's, the design chart for 50 Ω direct matching is not expected to be as good as the one in Figure 8. In fact, commercial biconical antennas typically have a matching circuit to compensate that.

The availability of a closed-form solution for the impedance of the SCCA (or its biconical counterpart) surely eases the generation of design charts such as the proposed. Nonetheless, the rationale still applies to other variants of the conical antenna, such as the skeleton biconical antenna [11, 12] or the OCA, provided the impedance estimates needed in step (i) are obtained otherwise. They could be derived by measurements or from antenna analysis software simulations. Actually, more realistic design charts are expected to be generated this way, since theoretical models usually disregard a few practical aspects. In this sense, the next section presents design charts for the OCA based on simulations from CST MW Studio, including the influence of another important geometrical parameter, the feed gap length.

4. Open Conical Antenna Design

4.1. Outline. The OCA configuration, depicted in Figure 9, is actually easier and cheaper to assemble than the SCCA. Since the opening is in line with the axial direction and recalling that the radiation intensity towards the z-axis is inherently low in relation to the horizontal plane, as assessed in [3, 6], the OCA tends to perform very similarly to the SCCA, either impedance-wise or radiation-wise.

In order to apply the design chart procedure of Section 3 to a more realistic configuration, impedance estimates of the OCA were derived with the aid of CST MW Studio. In addition, the simulations incorporated the feed gap influence

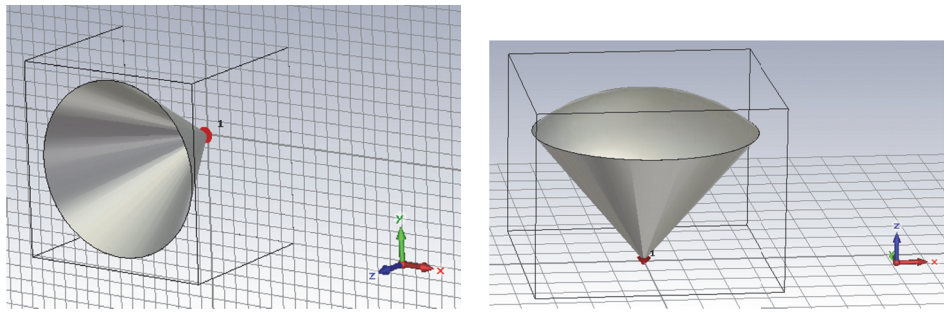

(a) (b)

Figure 10: CST GUI views of the (a) OCA and (b) SCCA.

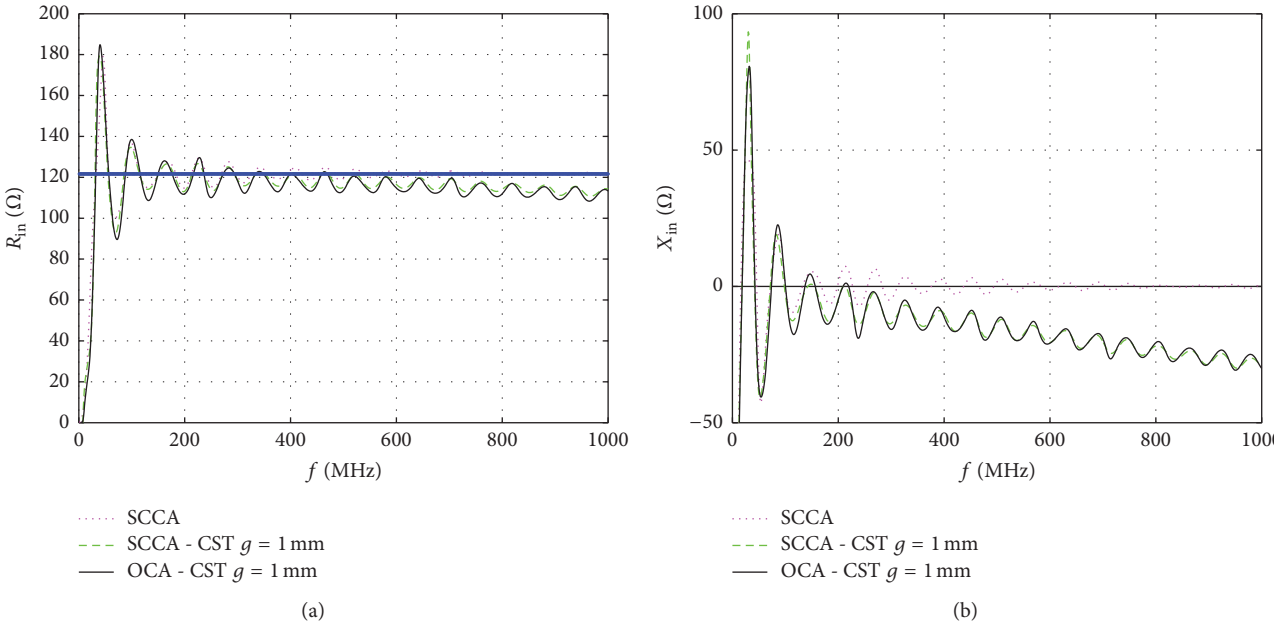

(a) (b)

Figure 11: Z_{in} of the theoretical SCCA and the CST simulated SCCA and OCA for $\theta_0 = 15^\circ$: (a) R_{in} and (b) X_{in}.

on the impedance. In the theoretical model of the SCCA in [5, 6], the gap length g was assumed to be infinitesimally small, and for that its influence was not assessed.

Both SCCA and OCA configurations were simulated in CST for $N = 15$ flare angles: $\theta_0 = 10^\circ, 15^\circ, 20^\circ, \ldots, 80^\circ$. Figure 10 reproduces the SCCA and OCA views from the graphical user interface (GUI) of CST. The design requirements were the same from the example in Section 3: $Z_r = 50\,\Omega$, S_{11} thresholds at −6 and −10 dB, $a = 2.5$ m, $f_{max} = 1$ GHz, and $f_H/f_L > 20$. PEC antennas were considered.

The CST setup for simulation was similar to the ones adopted in [13, 14]. The ground plane was set as PEC and a 50 Ω discrete port was inserted between the cone and the plane. Also, the ground plane was assumed to be perfect, extending to infinity, which is achieved setting xy plane boundary condition to be a PEC. The minimum gap length from which the time domain solver was able to provide valid results was $g = 1$ mm. The cone shell width w of the OCA was set to 0.5 mm. Mesh size varied from 20 to 26 cells per wavelength (of the maximum frequency, 1 GHz). The solver precision was equal to or better than −60 dB. The frequency span was from 1 MHz to 1 GHz, with 1000 samples.

4.2. SCCA versus OCA. Figures 11–13 present the SCCA and OCA impedances calculated from CST at the same three different flare angles of Section 2: 15°, 45°, and 75°. They also show the corresponding theoretical estimate for the SCCA for comparison purposes. As expected, the OCA impedance does not differ much from the SCCA, indicating that the cap effect is not that significant. What seems to be more relevant in the present comparison is the feed gap effect, present only in the simulated curves. It imposes an almost linear tilt to Z_0 convergence line in R_{in} curves, as well as to $X = 0$ line, which represents the convergence reactance value of the theoretical X_{in}. Such effect surely deserves a detailed analysis regarding the angle dependence, but it is out of the scope of the present

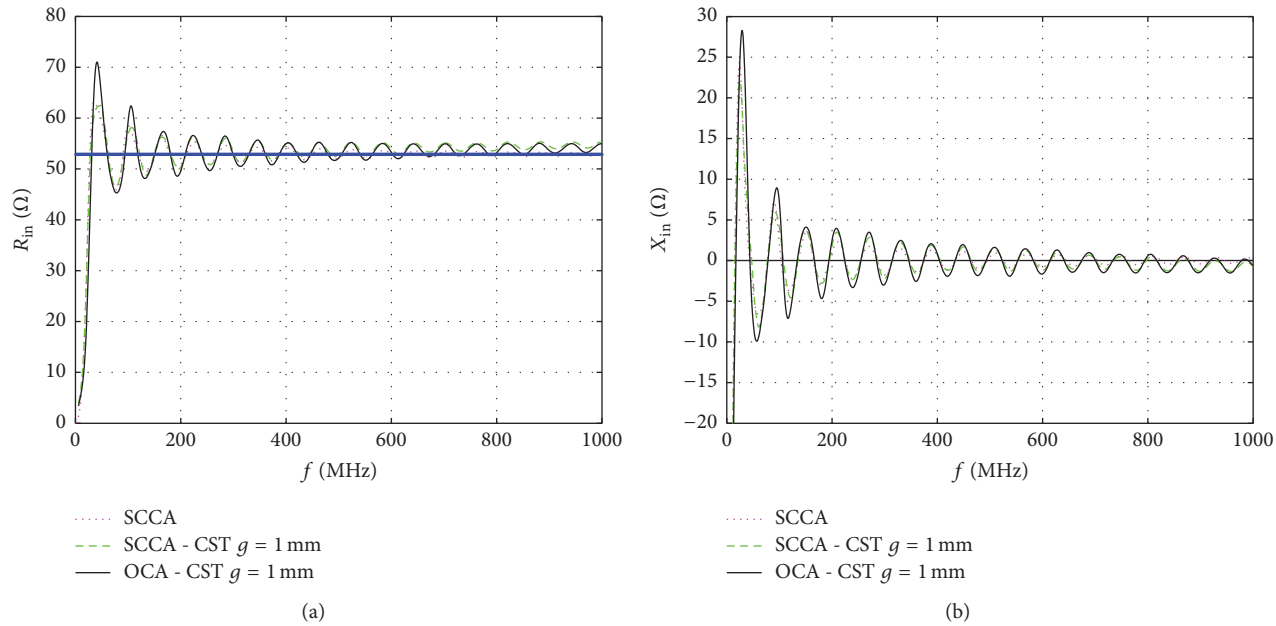

FIGURE 12: Z_{in} of the theoretical SCCA and the CST simulated SCCA and OCA for $\theta_0 = 45^\circ$: (a) R_{in} and (b) X_{in}.

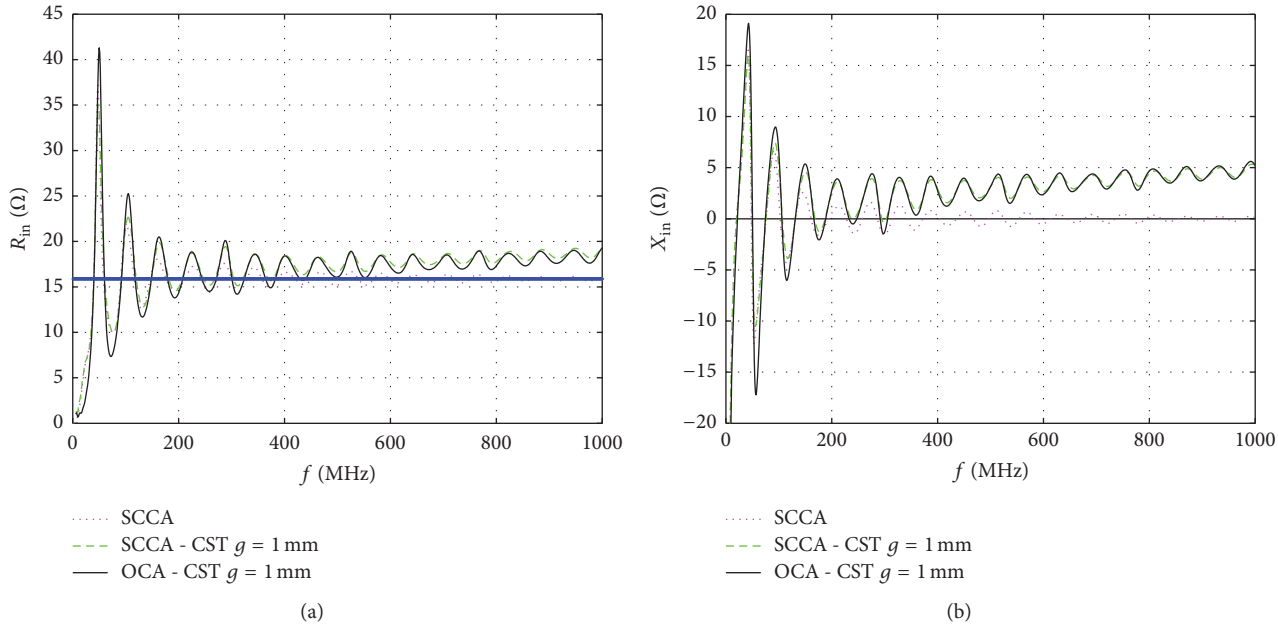

FIGURE 13: Z_{in} of the theoretical SCCA and the CST simulated SCCA and OCA for $\theta_0 = 75^\circ$: (a) R_{in} and (b) X_{in}.

work. It is worth mentioning that an unsuccessful attempt to fit such effects to a lumped RLC circuit model was made, but the results clearly indicated that a more complex approach is needed.

The corresponding reflection coefficients for the present example are shown in Figures 14–16. Though the tilt due to the feed gap is more clearly seen at the highest frequencies, the most relevant impact in this sense is on the passband lower limit f_L definition. Such behavior is better evidenced in $f_L \times \theta_0$ chart in Figure 17. As a consequence, the broadband potential of the more realistic conical antennas is lower than the one predicted by the theoretical model, as seen in $f_H/f_L \times \theta_0$ chart in Figure 18. It is also worth noting that the cap effect is also more relevant at the lower part of the spectrum, as seen in

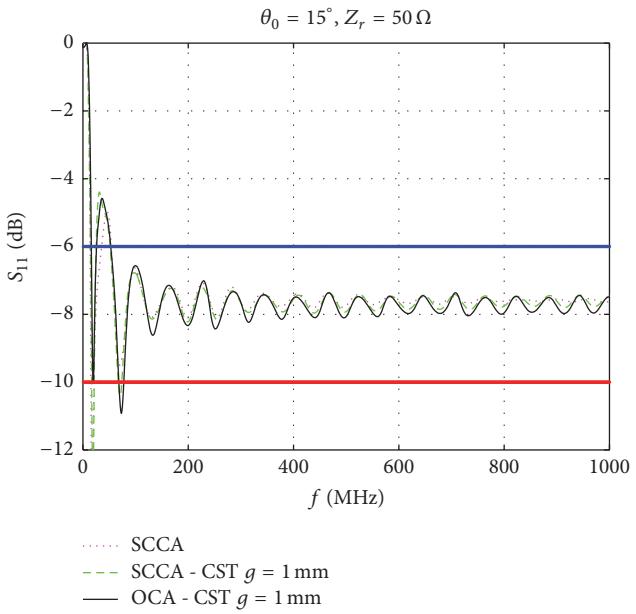

Figure 14: S_{11} of the theoretical SCCA and the CST simulated SCCA and OCA for $\theta_0 = 15^\circ$ and $Z_r = 50\,\Omega$.

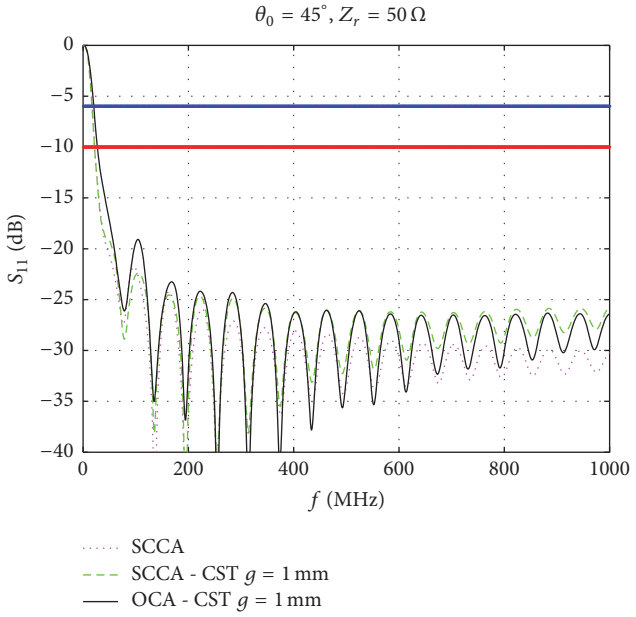

Figure 15: S_{11} of the theoretical SCCA and the CST simulated SCCA and OCA for $\theta_0 = 45^\circ$ and $Z_r = 50\,\Omega$.

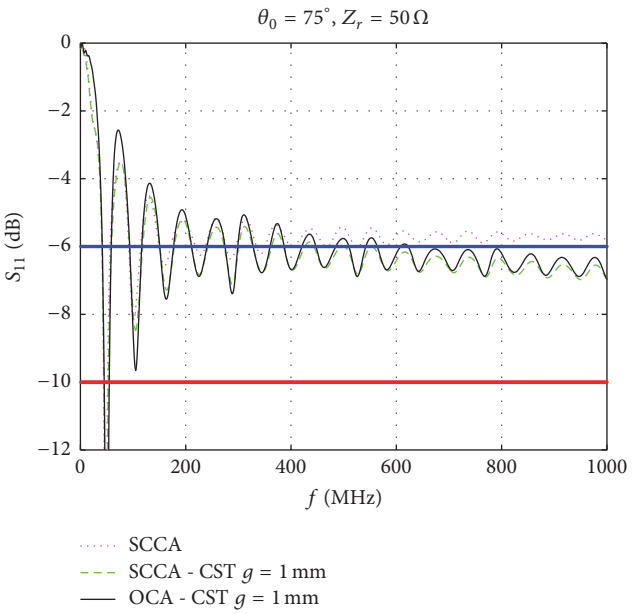

Figure 16: S_{11} of the theoretical SCCA and the CST simulated SCCA and OCA for $\theta_0 = 75^\circ$ and $Z_r = 50\,\Omega$.

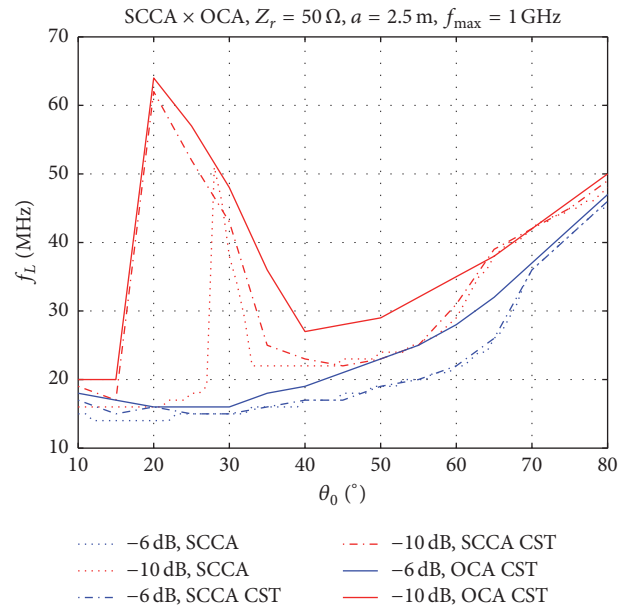

Figure 17: $f_L \times \theta_0$ chart for the theoretical SCCA and the CST simulated SCCA and OCA for $Z_r = 50\,\Omega$.

the charts of Figures 17 and 18, with the better performance of the SCCA over the OCA, as should be expected from wideband antennas fundamentals [1–3]. Finally, design charts for the simulated SCCA and OCA configurations are shown in Figures 19 and 20, reflecting the effects discussed so far. The same $DF_{min} = 20$ reference level of the previous section example was taken here.

4.3. Feed Gap Influence. The previous analysis pointed out the gap feed length as a relatively more impacting parameter than the spherical cap. Though the relevance of the feed gap to the conical antenna impedance and radiation performances should be expected, as addressed in [14], its dominance over the cap was not foreseen beforehand.

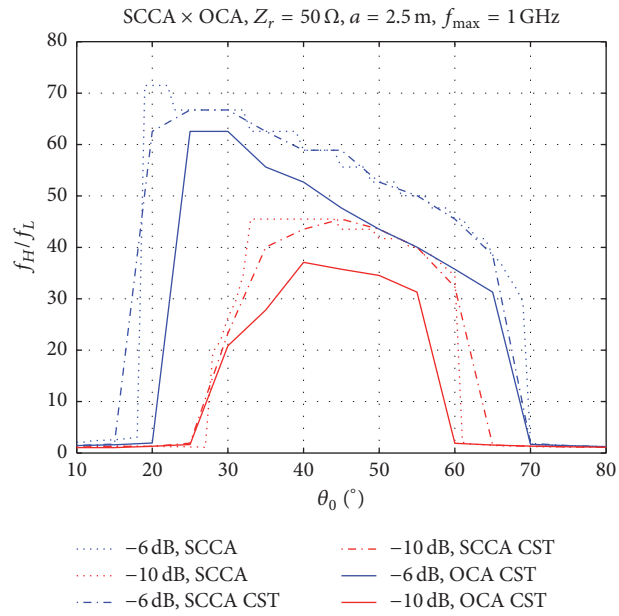

FIGURE 18: $f_H/f_L \times \theta_0$ chart for the theoretical SCCA and the CST simulated SCCA and OCA for Z_r = 50 Ω.

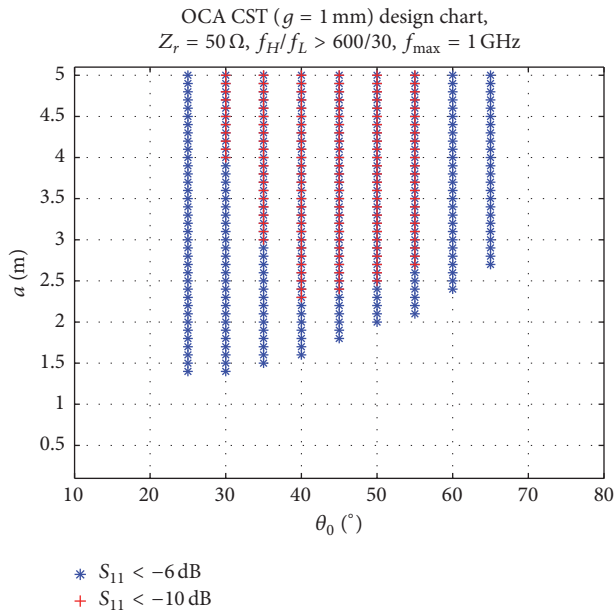

FIGURE 20: Design chart for the CST simulated OCA example with DF_{min} = 20.

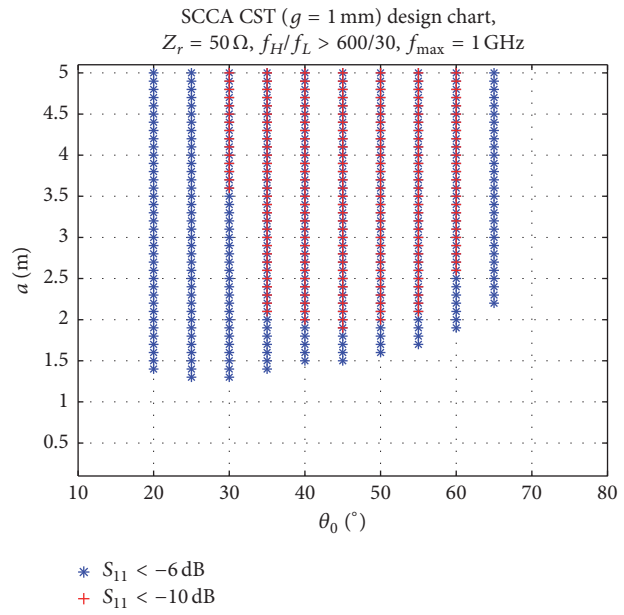

FIGURE 19: Design chart for the CST simulated SCCA example with DF_{min} = 20.

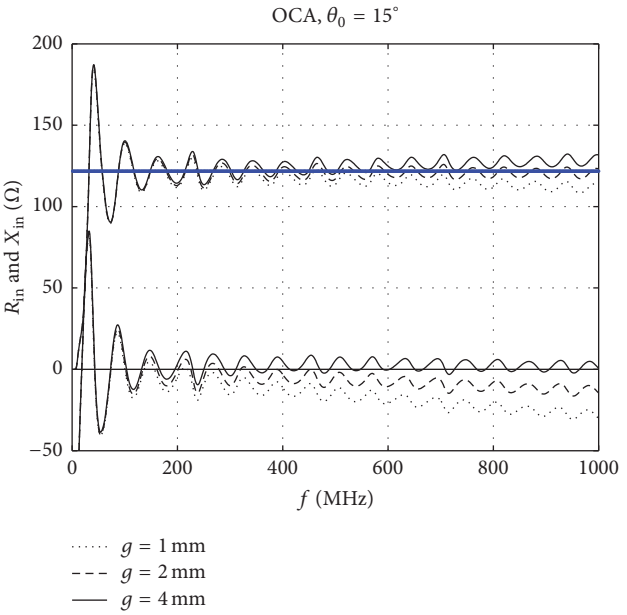

FIGURE 21: Z_{in} of the OCA for 3 different gap lengths and θ_0 = 15° (R_{in}: curves above, X_{in}: curves below).

In this sense, an extension to the feed gap analysis was carried out for the OCA configuration, calculating the impedance for two further gap lengths: 2 and 4 mm. Figures 21–23 show the impedance for the same three flare angles of the previous example. Though the most visible trend difference is the tilt at higher frequencies, the lower frequency band is also affected increasingly with longer gaps. The corresponding S_{11} curves in Figures 24–26 give the same impression.

The actual impact on the broadband performance is seen in the intermediary design charts in Figures 27 and 28. At least for the design requirements considered, the higher frequency tilt is still not enough to make $f_H < f_{max}$, as seen in Figure 27. On the other hand, f_L is pushed above for increasing gap lengths. Anyway, the overall impact on the relative bandwidth chart is low, as seen in Figure 28, not enough to inhibit the broadband potential of the OCA.

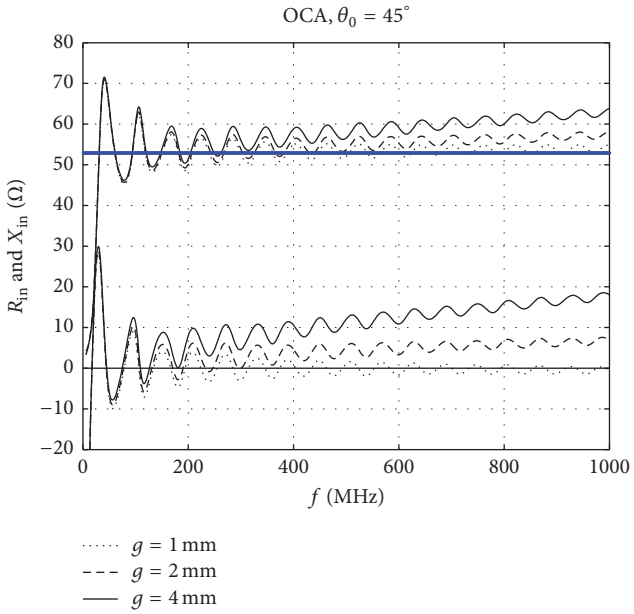

FIGURE 22: Z_{in} of the OCA for 3 different gap lengths and $\theta_0 = 45^\circ$ (R_{in}: curves above, X_{in}: curves below).

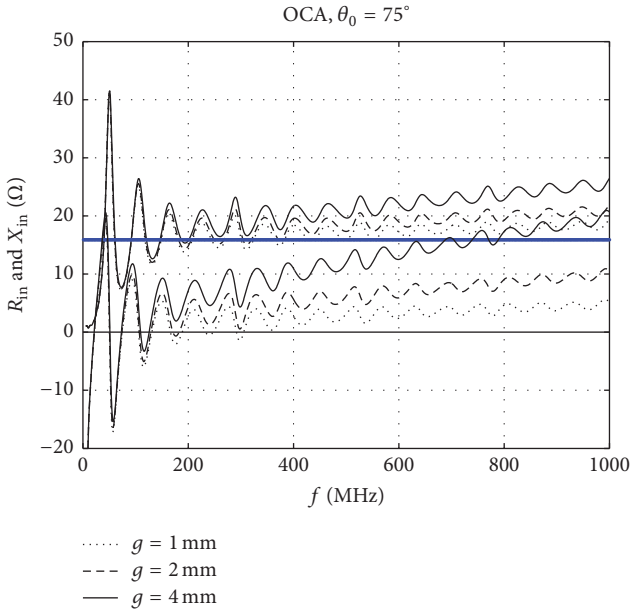

FIGURE 23: Z_{in} of the OCA for 3 different gap lengths and $\theta_0 = 75^\circ$ (R_{in}: curves above, X_{in}: curves below).

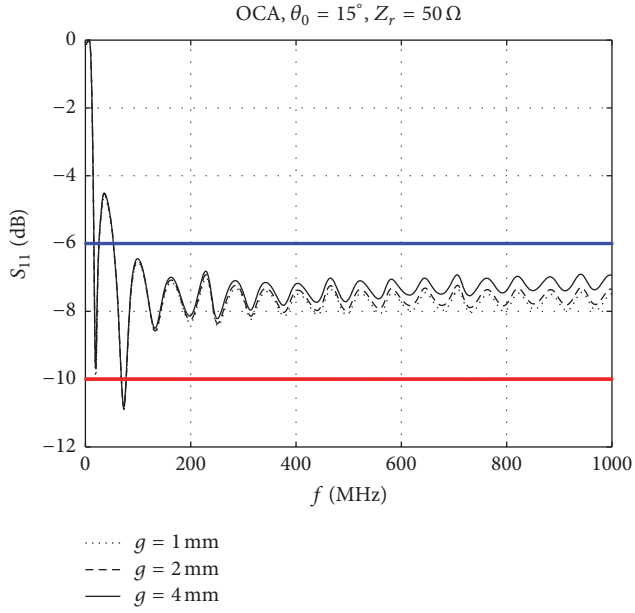

FIGURE 24: S_{11} of the OCA for 3 different gap lengths, $\theta_0 = 15^\circ$ and $Z_r = 50\,\Omega$.

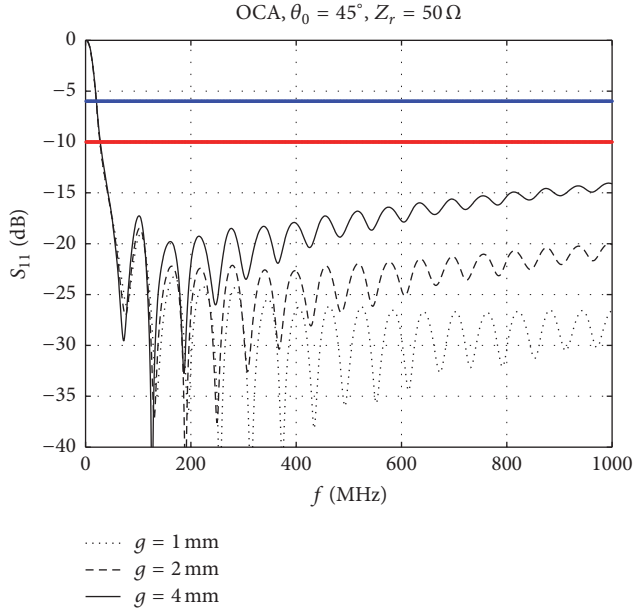

FIGURE 25: S_{11} of the OCA for 3 different gap lengths, $\theta_0 = 45^\circ$ and $Z_r = 50\,\Omega$.

5. Conclusion

In this paper, a 10-step sequence was proposed to derive charts that directly relate impedance matching bandwidth compliance to the main geometrical parameters of conical or biconical antennas. The motivation came from the challenge faced by the antenna engineer when specific broadband impedance requirements are imposed. From the design perspective, the choice for the conical or biconical configuration leads to the subsequent questions on how long and how opened must the antenna be to meet the specifications. The proposed charts try to provide straightforward answers to those queries.

The method was assessed taking the SCCA and the OCA configurations, using theoretical and simulated estimates of

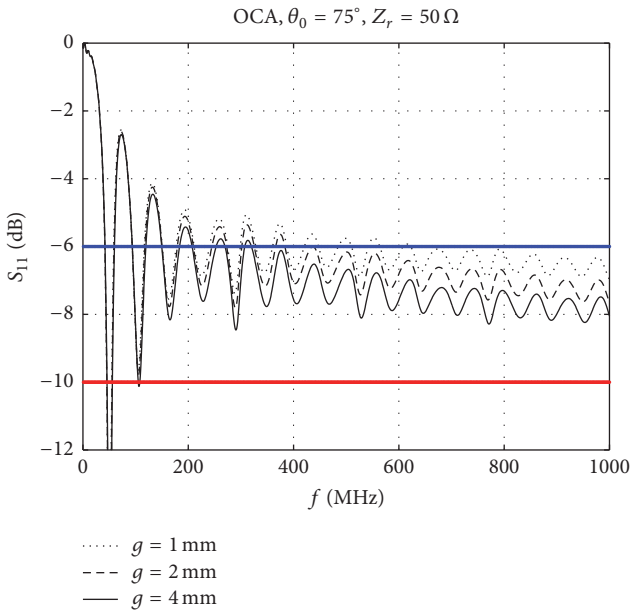

FIGURE 26: S_{11} of the OCA for 3 different gap lengths, $\theta_0 = 75^\circ$ and $Z_r = 50\,\Omega$.

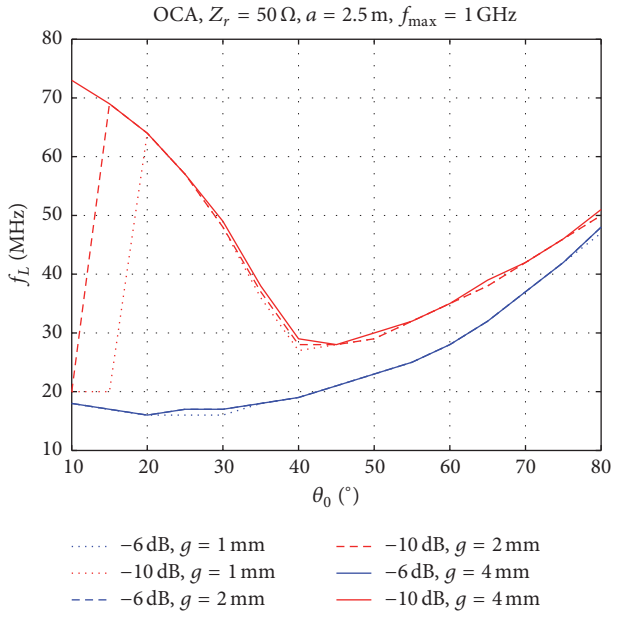

FIGURE 27: $f_L \times \theta_0$ chart for the OCA for 3 different gap lengths and $Z_r = 50\,\Omega$.

the input impedance. A hypothetical set of requirements was imposed, with a reference impedance of 50 Ω, −6 and −10 dB S_{11} thresholds, and a minimum relative bandwidth such that f_H/f_L was greater than 20. The impact of the spherical cap and the feed gap was also addressed, concluding that the broadband performance of those antennas is still achieved for a relatively large set of angles and lengths, as seen in the design charts.

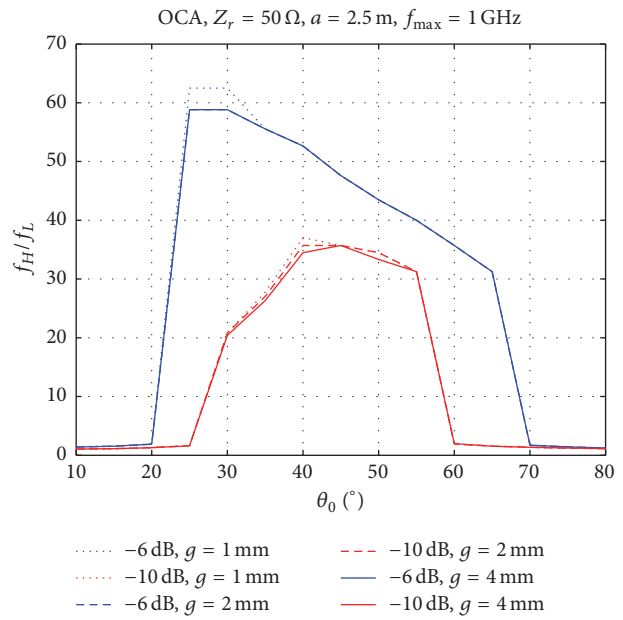

FIGURE 28: $f_H/f_L \times \theta_0$ chart for the OCA for 3 different gap lengths and $Z_r = 50\,\Omega$.

Competing Interests

The authors declare that there is no conflict of interests regarding the publication of this paper.

References

[1] C. A. Balanis, *Antenna Theory: Analysis and Design*, John Wiley & Sons, Hoboken, NJ, USA, 3rd edition, 2005.

[2] J. L. Volakis, *Antenna Engineering Handbook*, McGraw Hill, New York, NY, USA, 4th edition, 2007.

[3] S. A. Schelkunoff, "Ultrashort electromagnetic waves IV—guided propagation," *Electrical Engineering*, vol. 62, no. 6, pp. 235–246, 1943.

[4] P. D. P. Smith, "The conical dipole of wide angle," *Journal of Applied Physics*, vol. 19, no. 1, pp. 11–23, 1948.

[5] C. H. Papas and R. King, "Input impedance of wide-angle conical antennas fed by a coaxial line," *Proceedings of the IRE*, vol. 37, no. 11, pp. 1269–1271, 1949.

[6] C. H. Papas and R. King, "Radiation from wide-angle conical antennas fed by a coaxial line," *Proceedings of the IRE*, vol. 39, no. 1, pp. 49–51, 1951.

[7] S. S. Sandler and R. W. P. King, "Compact conical antennas for wideband coverage," *IEEE Transactions on Antennas and Propagation*, vol. 42, no. 3, pp. 436–439, 1994.

[8] S. N. Samaddar and E. L. Mokole, "Biconical antennas with unequal cone angles," *IEEE Transactions on Antennas and Propagation*, vol. 46, no. 2, pp. 181–193, 1998.

[9] D. Ghosh, T. K. Sarkar, and E. L. Mokole, "Design of a wide-angle biconical antenna for wideband communications," *Progress In Electromagnetics Research B*, vol. 16, pp. 229–245, 2009.

[10] D. A. McNamara, D. E. Baker, and L. Botha, "Some design considerations for biconical antennas," in *Proceedings of the*

International Symposium Digest-Antennas and Propagation, vol. 22, pp. 173–176, Boston, Mass, USA, June 1984.

[11] S. M. Mann and A. C. Marvin, "Characteristics of the skeletal biconical antenna as used for EMC applications," *IEEE Transactions on Electromagnetic Compatibility*, vol. 36, no. 4, pp. 322–330, 1994.

[12] O. Givati and A. P. C. Fourie, "Analysis of skeletal wire conical antennas," *IEEE Transactions on Antennas and Propagation*, vol. 44, no. 6, pp. 844–858, 1996.

[13] M. Gardill, "Receiving mode CST MWS/MATLAB co-simulations for time and frequency domain UWB small antenna array characterization," in *Proceedings of the CST European User Conference*, Stuttgart, Germany, April 2013.

[14] R. Kudpik, K. Meksamoot, N. Siripon, and S. Kosulvit, "Design of a compact biconical antenna for UWB applications," in *Proceedings of the 19th IEEE International Symposium on Intelligent Signal Processing and Communications Systems (ISPACS '11)*, pp. 1–6, IEEE, Chiang Mai, Thailand, December 2011.